Sensors and Materials, Vol. 35, No. 12 (2023) 4235–4250
MYU Tokyo

S & M 3478

Identification of Influential Factors in the Development of Modified Screen-printed Carbon Electrode in the DNA-based Electrochemical Biosensor Using the Design of Experiment

Muflihah,[1,2] Ari Hardianto,[1] Irkham,[1] Salma Nur Zakiyyah,[1]
Pintaka Kusumaningtyas,[2] Sulistyo Prabowo,[3] and Yeni Wahyuni Hartati[1*]

[1]Department of Chemistry, Faculty of Mathematics and Natural Sciences, Universitas Padjadjaran, Bandung 45363, Indonesia
[2]Chemistry Education Study Program, Faculty of Teacher Training and Education, Universitas Mulawarman, Samarinda 75119, Indonesia
[3]Department of Agricultural Products Technology, Universitas Mulawarman, Samarinda 75119, Indonesia

(Received November 9, 2023; accepted December 11, 2023)

Keywords: design of experiment, biosensor, ssDNA probe, screen-printed carbon electrode, gold nanoparticle

Over the last decade, many applications of electrochemical sensors/biosensors have been developed with various considerations such as cost-effectiveness, process simplicity, high sensitivity and accuracy, the need for the amount of analyte, and a miniature structure with portability. Until now, various electrochemical methods have been used to develop biosensors for detecting molecular markers, especially their modifications with nanoparticles. Historically, gold is a very inert material with little or no reactivity; thus, nanosized gold particles have been shown to function as an effective catalyst for a number of chemical reactions under various experimental conditions. In this study, the design of experiment (DoE) is used to create a model and analyze the best response that is affected by several independent variables with the aim of optimizing the response. The results showed that gold nanoparticles (AuNPs) were able to increase the peak current on the screen-printed carbon electrode-gold nanoparticle electrode and produced two of the most significant factors, namely, the concentration of single-stranded deoxyribonucleic acid (ssDNA) probe and the attachment time of AuNPs.

1. Introduction

A biosensor method involves the use of biomolecules such as enzymes, DNA, proteins, antibodies, and whole cells as sensing elements. These biomolecules interact with the analyte through a chemical reaction facilitated by a transducer, which converts chemical energy into an electrical signal. The signal is then processed by electronic circuits to obtain a usable output.(1) One advantage of this method is the ability to quickly measure a variety of targets, including biomolecules, at a low cost. Biosensors can be designed with different types of transducers,

*Corresponding author: e-mail: yeni.w.hartati@unpad.ac.id
https://doi.org/10.18494/SAM4773

ISSN 0914-4935

including electrochemical and optical transducers, which are preferred owing to their advantageous characteristics.[1] The quality and specificity of a biosensor depend on the biochemical specificity of the biomolecule and the transducer quality. Immobilization methods and support materials play a crucial role in the performance of biosensors.[2] Overall, biosensors offer a promising approach for various applications in the medical, environmental, and food industries.[1,2]

In the DNA-based electrochemical biosensor method, the important components include the electrode used, the bioreceptor compound, the bioreceptor immobilization on the electrode surface, and the detection process. The choice of the appropriate immobilization technique is crucial for producing an efficient, simple, and inexpensive biosensor. Several immobilization techniques such as adsorption, covalent bonding, cross-linking, and encapsulation can be used. The immobilization of biological elements should provide stability, allow for the diffusion of substrates and products, and enable excellent electron transfer. The immobilization method plays a significant role in the operational and storage stability of the biosensor.[3] The immobilization of enzymes onto the electrode surface not only affects enzyme activity but also maintains the structural integrity of the enzyme, which is important for the overall performance of enzymatic biosensors.[4] The immobilization technique should be reproducible, simple, cost-effective, and have a short processing time.[5]

In this study, we aim to select the determinants of measurement accuracy using the biosensor method including the following factors: gold nanoparticle (AuNP) volume, AuNP incubation time, measurement potential range, the concentration of the single-stranded deoxyribonucleic acid (ssDNA) probe, the immobilization incubation time of the ssDNA probe, $AgNO_3$ concentration, $NaBH_4$ concentration, $NaBH_4$ soaking time, Ag electrodeposition potential, and Ag deposition time. We used the design of experiment (DoE) to identify the most influential among these factors. The DoE approach offers several advantages over the one-factor-at-a-time (OFAT) approach. First, DoE allows for the simultaneous evaluation of multiple factors and their interactions, providing a more comprehensive understanding of the system. This contrasts with OFAT, which only considers one factor at a time while keeping others constant. Secondly, DoE reduces the number of experimental runs required compared with OFAT, making it more efficient and cost-effective. Thirdly, DoE enables the development of statistical models that can accurately predict the response on the basis of the input factors, allowing for the optimization and prediction of optimal conditions. This is particularly useful in complex systems where multiple factors affect the response.[5] Overall, DoE provides a systematic and efficient approach for studying the effects of multiple factors and their interactions, leading to the improved understanding and optimization of processes.[5,6]

2. Data, Materials, and Methods

2.1. Materials

The materials used included thiol-probe ssDNA (5'ACAATTTICCCCCAICITTAI) (Bioneer), demineralized water (PT Ikapharmindo Putramas, Jakarta, Indonesia), screen-printed carbon

electrode (SPCE) (Zimmer and Peacock), chloroauric acid ($HAuCl_4 \cdot 3H_2O$) (synthesized in 2020 at the Laboratory of Chemical Analysis and Separation), acid sulfate (H_2SO_4) (Merck, Germany), potassium ferricyanide $K_3[Fe(CN)_6]$ (Merck, Germany), potassium chloride (KCl) (Merck, Germany), sodium hydroxide (NaOH) (Merck, Germany), $AgNO_3$ (Sigma, US), $NaNO_3$ (Merck, Germany), $NaBH_4$ (Merck, Germany), NaCl (Merck, Germany), nuclease-free water (NFW) (Merck, Germany), phosphate-buffered saline (PBS) (Sigma, US), saline-sodium citrate (Merck, Germany), trisodium citrate ($Na_3C_6H_5O_7 \cdot 2H_2O$) (Merck, Germany), and Tris (2-carboxyethyl) phosphine (TECP) (Merck, Germany).

2.2 Methods

2.2.1 Preparation of colloidal AuNPs

We pipetted 145.7 μL of 51.49 mM chloroauric acid solution into an Erlenmeyer flask and diluted it with demineralized water up to 10 mL, followed by stirring over a magnetic stirrer and heating until boiling. After boiling, 1.7 mL of 1% trisodium citrate was added and stirred while heating until the color of the solution changed to red wine. The solution obtained was transparent red. Then, the colloidal nanoparticles that had been prepared were stored in a brown glass bottle at 4 °C. After that, the colloidal gold nanoparticles formed were characterized using a UV-Vis spectrophotometer.[7,8]

2.2.2 Modification of SPCE/AuNPs

SPCE generally consists of several parts, namely, base substrates, a working electrode (WE) made of carbon, Ag/AgCl as the reference electrode (RE), a carbon-based counter electrode (CE), and insulator ink materials (dielectric). SPCE was dripped with 15.0 μL of AuNP colloid solution and left for 24 h to dry. The modified SPCE was rinsed with mineralized water. Electrochemically modified SPCE gold nanoparticles were characterized by differential pulse voltammetry (DPV) using a redox system of 10 mM $K_3[Fe(CN)_6]$ solution in 0.1 M KCl over a potential range from −0.8 to +0.8 V at a scan rate of 0.008 V/s, with E_{step} of 0.005 V, E_{pulse} of 0.05 V, and t_{pulse} of 0.05 s. SPCE before and after modification was characterized by scanning elektron microscope (SEM).[9,10]

2.2.3 Immobilization of ssDNA probes on SPCE/AuNP

The gold-SPCE was rinsed with demineralized water; then, 5 μL of thiolated ssDNA probe with a concentration listed in Table S1 (dissolved with TCEP) was dropped onto the electrode surface and incubated for a specific time tabulated in Table S1. After the immobilization was complete, the SPCE/AuNP/ssDNA probe was rinsed 5 times using a buffer solution of SSC pH 7.0.[11]

2.2.4 Ag measurement

After combining 20 μL of $AgNO_3$ and 20 μL of $NaNO_3$, we coated the SPCE-Au ssDNA probe with the mixture and rinsed it with PBS. We measured the Ag using DPV after adding 40 μL of $NaBH_4$, rinsing (washing off) with PBS, and adding 20 μL of NaCl and 20 μL of $NaNO_3$.

2.2.5 Determination of influential factors

Plackett-Burman design[12] was used as the initial step to roughly screen influential factors in the development of the modified SPCE in the ssDNA-based electrochemical biosensor. Two-level fractional factorial design was employed to further refine the screening results. A full factorial design was utilized when the data analysis from the two-level fractional factorial experiment results still gave more than three screened factors and a confusing conclusion in terms of influential factors and their interactions. The factors included AuNP solution volume, AuNP incubation time, potential DPV range, ssDNA probe-SH concentration, the immobilization incubation time of the ssDNA probe, $AgNO_3$ concentration, $AgNO_3$ holding time, $NaBH_4$ concentration, $NaBH_4$ immersion time, Ag electrode potential, and deposition time.

2.2.6 Data analysis

The resulting current responses from DoEs were analyzed using main effect plots and the analysis of variances (ANOVA). Data analyses were performed using a FrF2 package[13] of R programming language[14] in a Jupyter Notebook[15] as an integrated development environment.

3. Results and Discussion

3.1 Characterization of colloidal AuNPs

The use of nanoparticles is one of the methods used in the development of a biosensor. AuNPs have a suitable function to increase the sensitivity and selectivity of biosensors owing to their relatively simple biocompatibility and optical, electronic, production, and modification properties.[16]

AuNPs exhibit a high surface area ratio and excellent conductivity. Owing to their large surface area, AuNPs are used for biomolecular recognition at interfaces through the transduction of electrochemical signals and the amplification of the resulting electrical responses. AuNPs are widely used in the development of biosensors because they can catalyze electrochemical reactions, can be used for labeling molecules, and can provide conditions suitable for the immobilization of biomolecules so as to facilitate electron transfer.[16,17] AuNPs have the ability to enhance the detection signal and electron transfer and can bind specifically and strongly to compounds containing sulfur.[18]

The Turkevich method[19] was first introduced in 1951 and is one of the most commonly used methods for the synthesis of AuNPs, which is based on the reduction of the precursor

tetrachloroauric acid with trisodium citrate in a boiling water solution. The colloidal gold nanoparticles are shown in Fig. 1.

Gold oxidation numbers include Au^{+} (aurous) and Au^{3+} (auric/auric), and those that are not oxidized are Au^{0}, which is the final condition required for a nanoparticle. Therefore, the basic principle of this method involves the reduction of Au^{3+} to Au^{0} in the presence of a reducing agent such as trisodium citrate. The precursor chosen was chloroauric acid, where gold is in the oxidation state of Au^{3+},[16,20,21] while trisodium citrate functions as a stabilizing and reducing agent. Trisodium citrate electrostatically stabilizes gold nanoparticles. The negative charges of citrate ions adsorbed on the surfaces of the gold nanoparticles can prevent aggregation between nanoparticles owing to the repulsive force between the negative charges on the surfaces as shown in Fig. 2.[22,23]

The interaction of gold nanoparticles with visible light can be determined from the size, morphology, shape, and chemical environment of the synthesized nanoparticles. The resonance resulting from the oscillation of the electrons of the gold nanoparticles and the incident light waves gives the surface plasmon resonance of the gold nanoparticles. The surface plasmon resonance of the gold nanoparticles is in the wavelength range of 500–600 nm depending on the particle size.[24] The AuNP colloid

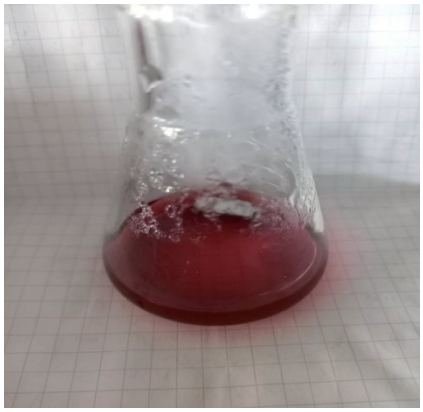

Fig. 1. (Color online) Colloidal gold nanoparticles (λ_{max} = 530 nm).

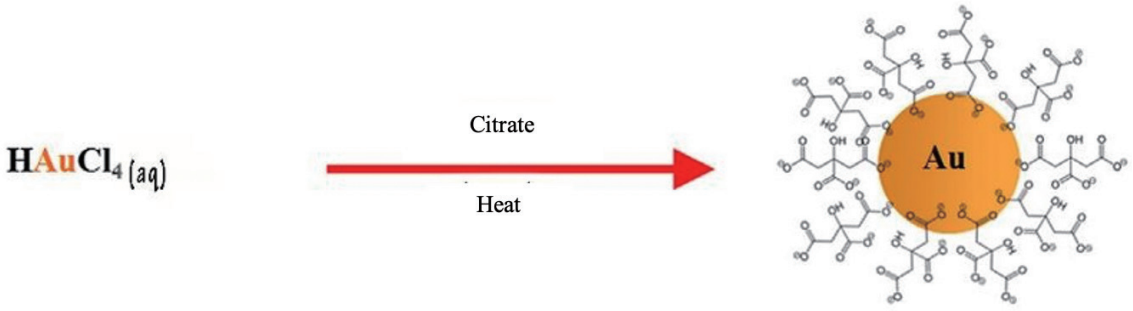

Fig. 2. (Color online) Synthesis of gold nanoparticles with trisodium citrate to reduce $HAuCl_4$.

produced in this study has an absorption peak at a wavelength with a maximum absorption (λ_{max}) of 530 nm [Fig. 3(a)], which indicates that the size is sufficiently small [Fig. 3(b)].

3.2 Immobilization of ssDNA probes on SPCE-Au

SPCE modification with gold aims to increase the sensitivity of SPCE because gold has high electrical conductivity, which contributes to electron transfer between the electrode surface and biomolecules, thereby increasing the sensitivity of the electrochemical sensor.[25,26] The selectivity of SPCE is increased by modifiying biorecognition molecules. Au interactions with thiolized biomolecules can produce strong bonds and improve the orientation of biorecognition molecules.[27]

The immobilization of biological molecules is one of the most important steps in biosensor development. The probe ssDNA is immobilized on the surface of the electrode so that it can hybridize with its complementary sequence. In this case, the nature of the electrode has a very important role. The interaction between gold on the surface of the electrode and thiol on the ssDNA probe forms a self-assembled monolayer (SAM), which is very important for optimal sensor design. A strong interaction (chemisorption) occurs between the thiolated ssDNA and the gold surface.[28] ssDNA on the gold electrode surface is often used due to the strong affinity interaction between the thiol groups and the gold surface to form Au-SH covalent bonds and a dense and regular monolayer.[29]

The S–Au reaction is a Lewis acid–base reaction, which is a reaction based on the bonding of free electrons from sulfur (S) atoms with Au. The reaction of S–Au occurs through the coordination of covalent bonds, which are bonds that occur between two or more atoms by sharing electrons. The S atom becomes positively charged because it binds to Au; to stabilize it, H^+ is released so that S becomes uncharged (tends to be stable). Au captures electrons from S so that AuO turns into Au^-. To stabilize Au^- to become AuO, electrons from Au^- are used to reduce H^+ to H_2, and SAMs are formed between Au and S.[30]

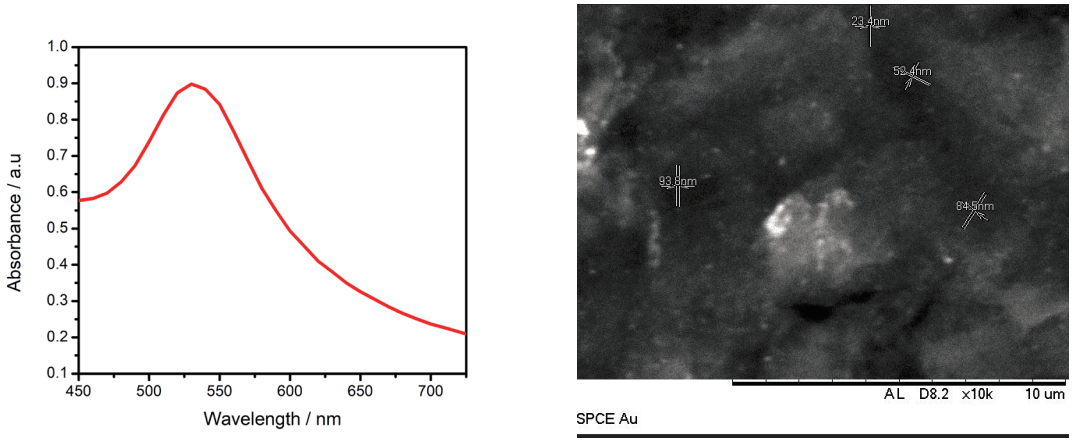

(a) (b)

Fig. 3. (Color online) Characterization of gold nanoparticles using (a) UV-Vis spectrophotometry and (b) SEM. The maximum absorption wavelength of gold nanoparticles is 530 nm.

Figure 4 shows the surface morphology of the electrochemical biosensor before and after modification as determined by SEM for bare SPCE, SPCE/AuNP and SPCE/AuNP/Probe.

The results of the characterization of the SPCE surface morphology before and after gold modification and after ssDNA probe immobilization showed significant differences in the SPCE surface before and after immobilization with gold. The initial SPCE appears smoother, even with uniform pores. Moreover, SPCE-Au has a rougher surface and there are small grains of gold particles that cover the electrodes evenly. Furthermore, the surface of SPCE-Au was seen to be more densely covered with small particles after ssDNA probe immobilization. The hybridization process will decrease in compliance with the increase in ssDNA density by AuNP because of the electrostatic repulsion produced by the negatively charged phosphate group from ssDNA.

3.3 Peaks of SPCE, SPCE-Au, and SPCE-Au-DNA probe

The results of peak current for SPCE before and after modification was characterized using DPV over a potential range of −0.5 to 0.5 V are shown in Table 1. SPCE-Au produces a higher peak current (17.822 μA) than the bare SPCE (11.340 μA) (Fig. 5). The gold attached to the SPCE surface facilitates electron transfer, thereby increasing the peak current (Fig. 6).

Figure 5(a) shows that SPCE was modified by AuNPs and that characterization using DPV revealed the redox system of the $K_3[Fe(CN)_6]$ solution in SPCE/AuNP (curve A) to exhibit an increase in peak current response. This is due to an increase in the conductivity of AuNPs by increasing electron transfer between electrodes. This indicates that the SPCE modification with AuNP has been successfully carried out. The electroactive nature of AuNPs increases the current response on the electrode surface so that the electrode can become more sensitive. In

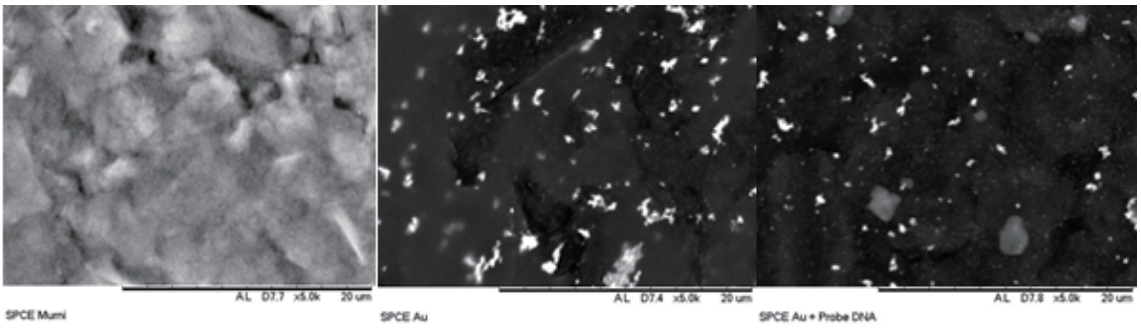

(a) (b) (c)

Fig. 4. Morphological characterization using SEM with 5000× magnification on (a) bare SPCE, (b) SPCE-Au, and (c) SPCE-Au with ssDNA probe.

Table 1
Current SPCE DPV characterization results and SPCE AuNP.

Current Measurement	Unmodified	Modified Au	Modified Au-DNA Probe
$K_3[Fe(CN)_6]$	11.340 μM	17.822 μM	14.779 μM

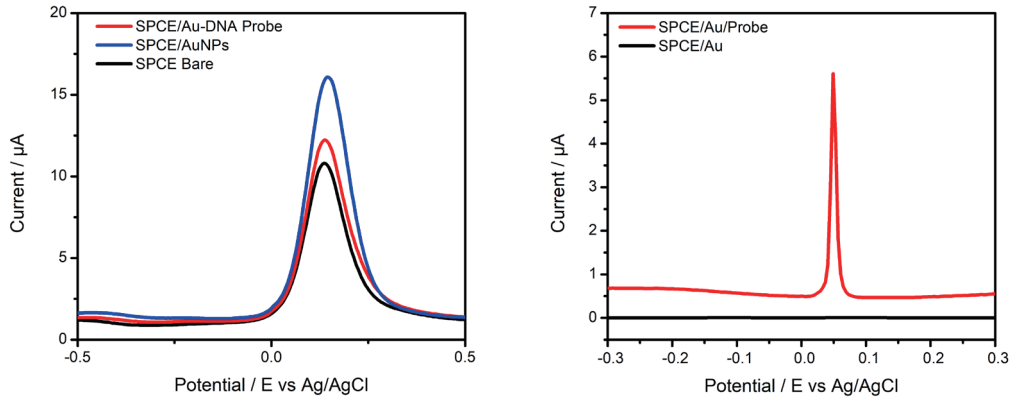

(a) (b)

Fig. 5. (Color online) Results of SPCE/AuNP differential pulse voltammogram characterization with (a) $K_3[Fe(CN)_6]$ and (b) Ag/AgCl.

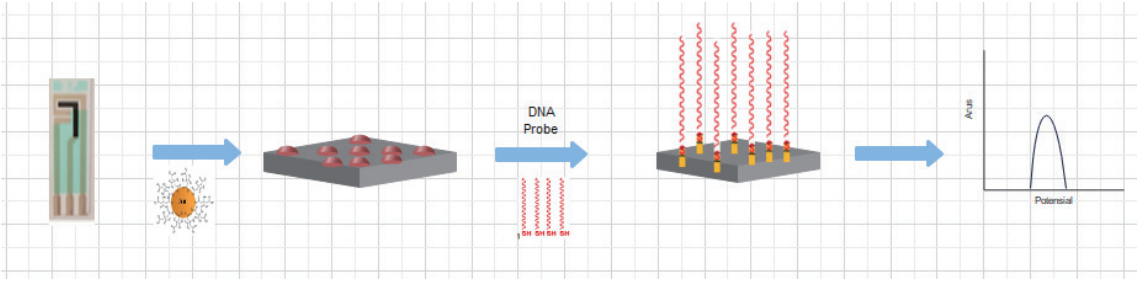

Fig. 6. (Color online) Schematic of immobilization of ssDNA probes on SPCE-Au.

Fig. 5(b), the measurement with Ag^+ shows a peak current at 0.05 V, which indicates the successful attachment of the metalized Ag to the ssDNA probe. This provides for greater sensitivity than previous methylene blue-based methods as silver is a more sensitive electroactive species and highly resilient once deposited on ssDNA. Importantly, these results were in good agreement with previous reports and could be explained by the strong electrostatic attraction between the negatively charged ssDNA and positively charged Ag^+.

3.4 Screening of influential factors using DoE

3.4.1 Plackett–Burman design

We listed ten potential influential factors in the development of SPCE-Au with the ssDNA probe. They are AuNP volume (A), DPV potential range (B), ssDNA probe concentration (C), the immobilization incubation time of the ssDNA probe (D), $AgNO_3$ concentration (E), $AgNO_3$ settling time (F), $NaBH_4$ concentration (G), $NaBH_4$ incubation time (H), Ag electrode potential

(I), and the duration of Ag electrodeposition (J). We used a Plackett–Burman design as the starting step to screen the ten potential factors shown in Table S1. This design is well suited for the initial screening of factors affecting a system, especially when the number of factors is large. A twelve-run experiment using the Plackett–Burman design can accommodate up to eleven factors.[31]

After conducting the experiments listed in Table S1. We analyzed the results using the main effect plot and the analysis of variance (ANOVA). The main effect plots (Fig. 7) and ANOVA (Table S2) indicate that AuNP volume (A), ssDNA probe concentration (C), $AgNO_3$ concentration (E), $AgNO_3$ settling time (F), and Ag electrode potential have significant decremental effects on the resulting current responses as their respective levels increase. The decremental impact of ssDNA probe concentration can be explained by the fact that a higher ssDNA concentration leads to an increased amount of ssDNA adhering to the modified SPCE, which may consequently increase the impedance. The decrease in current as the $AgNO_3$ concentration, $AgNO_3$ settling time, and Ag electrode potential increase may be due to several reasons. First, a silver layer formed on the electrode surface can act as a barrier, impeding electron transfer and resulting in a lower current response. Additionally, the silver layer formed from the reduction of Ag^+ ions can be nonconductive or semiconductive, especially if it is thick or not appropriatedly adhered to the electrode surface, leading to increased resistance and decreased current response. The competitive adsorption of Ag^+ ions with other species present in the solution can further affect the overall electrochemical response. These possibilities may collectively contribute to the observed decrease in current response with higher $AgNO_3$ concentrations.

On the other hand, the DPV potential range, the immobilization incubation time of the ssDNA probe, and the duration of Ag electrodeposition have incremental effects on the resulting current as their respective levels increase (Fig. 7). Nevertheless, statistical analysis reveals that only the DPV potential range (p-value = 4.9×10^{-8}, $\alpha = 5\%$) and the incubation period of ssDNA probe immobilization (1.7×10^{-6}) exert statistically significant impacts on the current response, as corroborated by Table S1. According to the experimental results derived from the Plackett–

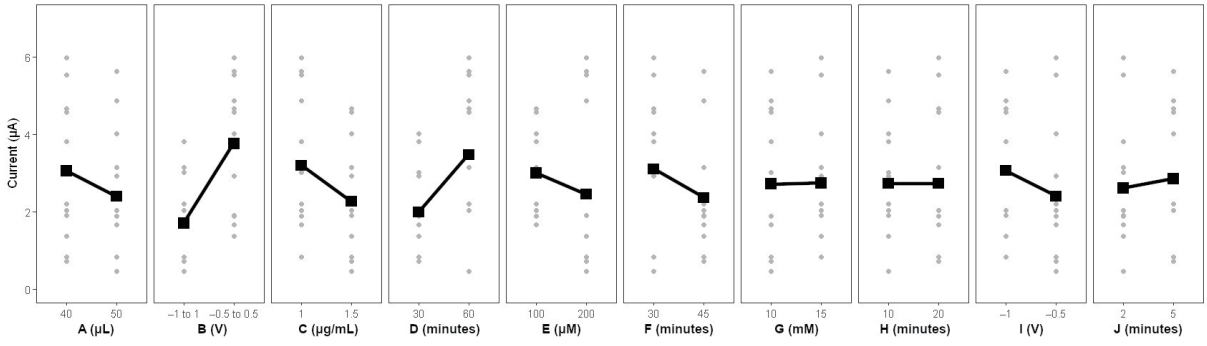

Fig. 7. Main effect plots from the experiment using the Plackett–Burman design. A is AuNP volume, B is DPV potential range, C is ssDNA probe concentration, D is the immobilization incubation time of the ssDNA probe, E is $AgNO_3$ concentration, F is $AgNO_3$ settling time, G is $NaBH_4$ concentration, H is the incubation time of $NaBH_4$, I is the potential applied to Ag electrodeposition, and J is the duration of Ag electrodeposition. Grey circle points are the current responses obtained from the experiment, whereas black square points denote the corresponding average values for each factor level.

Burman design, a more constrained DPV potential range is associated with an elevated current response. Moreover, the effect of the incubation duration on ssDNA probe immobilization exhibits a paradoxical correlation; a prolonged incubation duration may culminate in an increased quantity of immobilized ssDNA probe, consequently amplifying the impedance.

As shown in Fig. 7 and Table S2, the concentration and incubation time of $NaBH_4$ do not have a significant effect on factor current responses. This outcome may be attributable to the disparity in concentration scale between $NaBH_4$ and $AgNO_3$. Specifically, the low and high levels of $NaBH_4$ concentration are measured in millimolar (mM) units, which substantially exceed the micromolar (μM) concentration range of $AgNO_3$.

3.4.2 Two-level fractional factorial design

According to the analysis above on the experiment results using the Placket–Burman design, we found seven factors that may significantly affect the current response. They are AuNP volume, DPV potential range, ssDNA probe concentration, the immobilization incubation time of the ssDNA probe, $AgNO_3$ concentration, $AgNO_3$ settling time, and the potential applied to Ag electrodeposition. Nevertheless, it is important to note that the Plackett–Burman design ignores the interaction between factors. Any strong interaction between factors may lead to misleading interpretations.[12] Therefore, we reassessed the significant factors by conducting a set of follow-up experiments using the two-level fractional design, involving sixteen runs of resolution IV design (Table S3). The nonsignificant factors were set to constant levels, where the concentration and incubation time of $NaBH_4$ were 15 mM and 10 min, respectively, while the duration of Ag electrodeposition was 5 s.

The two-level fractional factorial experiment result exhibits main effect plots (Fig. 8) similar to those derived from the Plackett–Burman design (Fig. 7), except for the DPV potential range. On the basis of the findings from the Plackett–Burman experiment, narrowing the DPV potential range augments the current response. However, results from the two-level fractional factorial experiment indicate a converse effect, wherein narrowing the DPV potential range leads to a decline in current response. ANOVA (Table S4) suggests that the DPV potential range, ssDNA

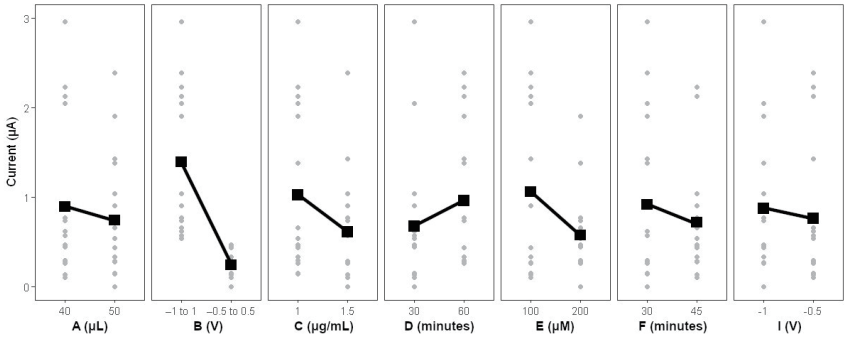

Fig. 8. Main effect plots from the experiment using a two-level fractional factorial design. A is AuNP volume, B is DPV potential range, C is ssDNA probe concentration, D is the immobilization incubation time of the ssDNA probe, E is $AgNO_3$ concentration, F is $AgNO_3$ settling time, and I is the potential applied to Ag electrodeposition. Grey circular data points represent the current responses obtained experimentally, while black square data points indicate the corresponding arithmetic mean values for each factor level.

probe concentration, and $AgNO_3$ concentration are significant factors affecting the current response, leaving the other four factors, namely, AuNP volume, the immobilization incubation time of the ssDNA probe, $AgNO_3$ settling time, and the electrode potential of Ag.

In voltammetric analyses, analyte ions in solution will move toward the surface of the electrode when the potential is released. The mechanism of mass transport/migration of ions from the solution to the electrode surface is by three ways, namely, convection, migration, and diffusion. Mass transport by convection is the transport of ions on the surface of the working electrode caused by stirring the solution and changes in temperature. Mass transport by migration is the transport of ions on the surface of the electrode caused by the movement of charged species from the electric field gradient. Migratory mass transport only affects the mass transfer of charged particles. Mass transport by diffusion is the transport of ions on the surface of the working electrode where there is spontaneous migration of the analyte from high concentration to low concentration. In the electrochemical analysis, the analyte is expected to move to the electrode surface by diffusion.[33] In this study, neither mechanical agitation nor heating was carried out on the measured SPCE. This precaution ensured that the applied electrode potential remained undisturbed, precluding any confounding effects on the measurement outcomes. Additionally, the volume of AuNP dispensed onto the SPCE surface was found to be inconsequential. This is attributed to the fact that both the 40 and 50 μL volumes were sufficient to envelop the entire SPCE surface, thereby facilitating a uniform coating of gold nanoparticles.

3.4.3 Two-level full factorial design

In the next stage, we performed a set experiment employing a two-level full factorial design to evaluate the interactions among the three significant factors identified in the preceding two-level fractional factorial experiment. The two-level full factorial design boasts superior resolution and concealed replication, yielding robust statistical power.[34] Additionally, this design incorporated the incubation duration for AuNPs as a new factor, which had been inadvertently omitted in the antecedent experimental configurations. Given four factors, the total number of experiments required for the two-level full factorial design is 16, as delineated in Table S5. For factors deemed statistically insignificant, their respective levels were configured to yield elevated current responses, as guided by the main effect plots in Fig. 8.

The two-level full factorial experiment results were then analyzed using the main effect plots (Fig. 9) and ANOVA (Table S6). The analysis results indicate that the concentration of the ssDNA probe significantly impacts the current response (p-value = 2.48×10^{-2}), which disagrees with the results of the analyses based on the Plackett–Burman and two-level fractional factorial experimental results. Interestingly, such ssDNA probe impact is consistent with previous studies highlighting the importance of probe concentration in biosensor performance.[35] An optimal concentration of the ssDNA probe is crucial for achieving high sensitivity and specificity in electrochemical biosensors.

The main effect plots (Fig. 9) and ANOVA (Table S6) also suggest that the incubation duration for AuNPs showed a significant positive impact on the current response (p-value = 2.64×10^{-2}). AuNPs are known to enhance the electrochemical signals owing to their high

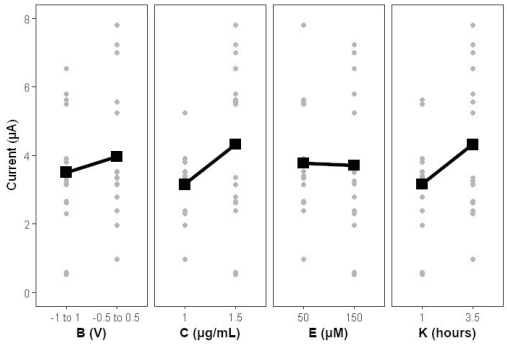

Fig. 9. Main effect plots from the experiment using a two-level fractional factorial design. B is DPV potential range, C is ssDNA probe concentration, E is $AgNO_3$ concentration, and K is the incubation duration for AuNP. Grey circular data points represent the current responses obtained experimentally, while black square data points indicate the corresponding arithmetic mean values for each factor level.

conductivity and large surface area. The incubation time allows for a higher adsorption of AuNPs on SPCE, thereby improving sensor performance.[35]

The longer the AuNPs are attached to SPCE, the more nanoparticles are expected to cover the surface of the electrode so that more ssDNA probe-SH will hybridize according to the increase in concentration.

Interestingly, the concentration of the ssDNA probe and the incubation duration for AuNPs showed a significant positive interaction affecting the current response with a p-value of 5.72×10^{-3} (Table S6). This p-value suggests that the combined effect of these two factors is greater than their individual effects. Optimizing the concentration of the ssDNA probe and the incubation time for AuNPs together can further enhance the biosensor performance.[36]

Another significant interaction was observed between the concentration of $AgNO_3$ and the incubation duration for AuNPs. $AgNO_3$ is commonly used for metalizing ssDNA probes, and its concentration can significantly affect the electrochemical properties of the sensor. The interaction with the incubation duration for AuNPs suggests that these two factors work together to optimize the biosensor performance.

5. Conclusions

The concentration of the ssDNA probe and the incubation duration for AuNs were identified as significant factors affecting the current response in the two-level full factorial experiment. Optimizing these factors can enhance the sensitivity and performance of the SPCE-based biosensor. Additionally, the interaction effects between the concentration of the ssDNA probe and the incubation duration for AuNPs, as well as between the concentration of $AgNO_3$ and the incubation duration for AuNPs, further improve the biosensor performance.

Acknowledgments

This work was supported by Padjadjaran University ALG Scheme No. 1549/UN6.3.1/PT.00/2023 (Yeni Wahyuni Hartati). Muflihah acknowledges the help from Indonesia's Ministry of Finance for the scholarship Beasiswa Pendidikan Indonesia No. 02694/J5.2.3./BPI.06/10/2022.

References

1 M. Asal, Ö. Özen, M. Şahinler, and İ. Polatoğlu: Sensors **18** (2018) 1924. https://doi.org/10.3390/s18061924
2 M. Asal, Ö. Özen, M. Şahinler, H. T. Baysal, and İ. Polatoğlu: Sens. Rev. **39** (2018) 377. https://doi.org/10.1108/SR-04-2018-0084
3 M. Singh, N. Verma, A. K. Garg, and N. Redhu: Sens. Actuators, B **134** (2008) 345. https://doi.org/10.1016/j.snb.2008.04.025
4 B. Wu, S. Hou, Y. Xue, and Z. Chen: Nanomaterials **8** (2018) 993. https://doi.org/10.3390/nano8120993
5 J. Gilman, L. Walls, L. Bandiera, and F. Menolascina: ACS Synth. Biol. **10** (2021) 1. https://doi.org/10.1021/acssynbio.0c00385
6 G. Hancu, S. Orlandini, L. A. Papp, A. Modroiu, R. Gotti, and S. Furlanetto: Molecules **26** (2021) 4681. https://doi.org/10.3390/molecules26154681
7 H. Shu, W. Wen, H. Xiong, X. Zhang, and S. Wang: Electrochem. Commun. **37** (2013) 15. https://doi.org/10.1016/j.elecom.2013.09.018
8 M. Roushani, Z. Jalilian, and A.Nezhadali: Heliyon **5** (2019) e01984. https://doi.org/10.1016/j.heliyon.2019.e01984
9 V. R. R. Bernardo-Boongaling, N. Serrano, J. J. García-Guzmán, J. M. Palacios-Santander, and J. M. Díaz-Cruz: J. Electroanal. Chem. **847** (2019) 113184. https://doi.org/10.1016/j.jelechem.2019.05.066
10 Y. W. Hartati, T. A. Setiawati, T. Sofyatin, F. Fitrilawati, A. Anggraeni, and S. Gaffar: ScienceAsia **46** (2020) 72. https://doi.org/10.2306/scienceasia1513-1874.2020.011
11 R. Nurmalasari, Yohan, S. Gaffar, and Y. W. Hartati: Procedia Chem. **17** (2015) 111. https://doi.org/10.1016/j.proche.2015.12.119
12 D. C. Montgomery: Design and Analysis of Experiments (John Wiley & Sons, Inc. 2019) 10th ed.
13 U. Grömping: Technometrics **56** (2014) 42. https://doi.org/10.1080/00401706.2013.822425
14 R Core Team. R: A Language and Environment for Statistical Computing 2019. https://www.r-project.org/
15 B. E. Granger and P. F. Jupyter: Comput. Sci. Eng. **23** (2021) 7. https://doi.org/10.1109/MCSE.2021.3059263
16 E. I. Fazrin, A. I. Naviardianti, S. Wyantuti, S. Gaffar, and Y. W. Hartati: PENDIPA J. Sci. Educ. **4** (2020) 21. https://doi.org/10.33369/pendipa.4.2.21-39
17 G. Favero, G. Fusco, F. Mazzei, F. Tasca, and R. Antiochia: Nanomaterials **5** (2015) 1995. https://doi.org/10.3390/nano5041995
18 K. Charoenkitamorn, O. Chailapakul, and W. Siangproh: Talanta **132** (2015) 416. https://doi.org/10.1016/j.talanta.2014.09.020
19 J. Polte , T. T. Ahner, F. Delissen, S. Sergey, F. Emmerling, A. F. Thunemann, and R. Kraehnert: J. Am. Chem. Soc. **132** (2010) 1296. https://doi.org/10.1021/ja906506j
20 M. Shah, V. Badwaik, Y. Kherde, H. K. Waghwani, T. Modi, and Z. P. Aguilar: Front. Biosci. **19** (2014) 1320. https://doi.org/10.2741/4284
21 C. Daruich De Souza, B. Ribeiro Nogueira, and M. E. C. M. Rostelato: J. Alloys Compd. **798** (2019) 714. https://doi.org/10.1016/j.jallcom.2019.05.153
22 X. L. Cheng, F. Wei, J. Chen , M.-H. Li, L. Zhang, Y.-Y. Zhao, and X.-Y. Xiao: J. Anal. Methods Chem. **2014** (2014) 764397. https://doi.org/10.1155/2014/764397
23 S. Wyantuti, R. A. Fadhilah, D. R. Eddy, and Y. W. Hartati: Chemica et Natura Acta **5** (2017) 65. https://doi.org/10.24198/cna.v5.n2.14608
24 S. A. Akintelu, S. C. Olugbeko, and A. S. Folorunso: Int. Nano Lett. **10** (2020) 237. https://doi.org/10.1007/s40089-020-00317-7
25 G. Lucarelli, F, Marrazza, A. P. F. Turner, and M. Mascini: Biosens. Bioelectron. **19** (2004) 515. https://doi.org/10.1016/S0956-5663(03)00256-2
26 N. Novianti, R. V. Manurung, and A. Arifin: Indonesian Journal of Electronics and Instrumentation Systems **10** (2020) 65. https://doi.org/10.22146/ijeis.54138
27 Y. W. Hartati, I. Irkham, I. Sumiati, S. Wyantuti, S. Gaffar, S. N. Zakiyyah, M. Ihda, and M. Ozsos: Biosensors **13** (2023) 657. https://doi.org/10.3390/bios13060657
28 C. Lorena and M. Palenzuela: TrAC, Trends Anal. Chem. **103** (2018) 110–118. https://doi.org/10.1016/j.trac.2018.03.016
29 B. Liu and J. Liu: Anal. Methods **9** (2017) 2633. https://doi.org/10.1039/c7ay00368d
30 K. M. Koo, A. A. I. Sina, L. G. Carrascosa, M. J. A. Shiddiky, and M. Trau: Analy. Methods **7** (2015) 7042. https://doi.org/10.1039/c5ay01479d
31 S. Wyantuti, F. W. Harahap, Y. W. Hartati, and M. L. Firdaus: J. Phys: Conf. Ser. **1731** (2021) 012017. https://doi.org/10.1088/1742-6596/1731/1/012017
32 Q. Zhao, M. Zhao, J. Qiu, W. Y. Lai, H. Pang, and W. Huang: Small **13** (2017) 1701091. https://doi.org/10.1002/smll.201701091

33 D. Harvey: DePauw U. Modren Analytical Chemistry. McGraw-Hill Higher Education. Published online (2000) 816.
34 J. Lawson: Design and Analysis of Experiments with R. Chapman and Hall (CRC, 2015). https://doi.org/10.1201/b17883
35 S. Dong, R. Zhao, J. Zhu, X. Lu, Y. Li, S. Qiu, L. Jia, X. Jiao, S. Song, C. Fan, R. Hao, and H. Song: ACS Appl. Mater. Interfaces **7** (2015) 8834. https://doi.org/10.1021/acsami.5b0143
36 B. Dalkıran, P. E. Erden, C. Kaçar, and E. Kılıç: Electroanalysis **31** (2019) 1324. https://doi.org/10.1002/elan.201900092

Supporting Information

Table S1
Plackett–Burman design for screening ten potential influential factors in the development of SPCE-Au with ssDNA probe. The ten factors include AuNP volume (A), DPV potential range (B), ssDNA probe concentration (C), the immobilization incubation time of the ssDNA probe (D), $AgNO_3$ concentration (E), $AgNO_3$ settling time (F), $NaBH_4$ concentration (G), the incubation time of NaBH4 (H), the electrode potential of Ag (I), and electrodeposition time (J). Every run was in duplicate resulting current as the response.

No	A	B	C	D	E	F	G	H	I	J	Current (μA)	
	(μL)	(V)	(μg/mL)	(min)	(μM)	(min)	(mM)	(min)	(V)	(s)	I	II
1	50	−1–+1	1.5	60	200	30	10	10	−0.5	2	0.676	0.727
2	50	−0.5–+0.5	1.5	30	100	30	15	10	−0.5	5	2.913	4.020
3	40	−0.5–+0.5	1.5	60	100	30	10	20	−1	5	4.121	4.649
4	50	−1–+1	1	30	200	30	15	20	−1	5	0.678	0.841
5	50	−0.5–+0.5	1	30	100	45	10	20	−0.5	2	1.679	1.893
6	40	−1–+1	1	60	100	45	15	10	-0.5	5	2.039	2.210
7	50	−1–+1	1.5	60	100	45	15	20	−1	2	2.040	3.141
8	40	−0.5–+0.5	1.5	30	200	45	15	10	−1	2	1.369	1.898
9	40	−1–+1	1	30	100	30	10	10	–1	2	3.008	3.821
10	40	−1–+1	1.5	30	200	45	10	20	−0.5	5	0.715	0.839
11	40	−0.5–+0.5	1	60	200	30	15	20	−0.5	2	5.533	5.981
12	50	−0.5–+0.5	1	60	200	45	10	10	−1	5	4.870	5.622

Table S2
Analysis of variance table from the regression of experiment results using the Plackett–Burman design in Table S1. The factors are AuNP volume (A), DPV potential range (B), ssDNA probe concentration (C), the immobilization incubation time of the ssDNA probe (D), $AgNO_3$ concentration (E), $AgNO_3$ settling time (F), $NaBH_4$ concentration (G), the incubation time of $NaBH_4$ (H), the electrode potential of Ag (I), and electrodeposition time (J). The factor e1 is a dummy variable in the Plackett–Burman design. Every run was in duplicate resulting current as the response.

	df	Sum Square	Mean Square	*F*-value	*p*-value
A	1	2.563	2.563	14.591	2.4×10^{-3}
B	1	25.205	25.205	143.488	4.9×10^{-8}
C	1	5.220	5.220	29.718	1.5×10^{-4}
D	1	13.185	13.185	75.063	1.7×10^{-6}
E	1	1.786	1.786	10.167	7.8×10^{-3}
F	1	3.251	3.251	18.507	1.0×10^{-3}
G	1	0.002	0.002	0.012	9.2×10^{-1}
H	1	0	0	0	9.9×10^{-1}
I	1	2.613	2.613	14.875	2.3×10^{-3}
J	1	0.343	0.343	1.955	1.9×10^{-1}
e1	1	15.933	15.933	90.706	6.1×10^{-7}
Residuals	12	2.108	0.176		

Table S3
Two-level fractional factorial design for the follow-up screening of seven potential influential factors in the development of SPCE-Au with ssDNA probe. The seven factors are from the initial factor screening using Plackett–Burman experiment (Table S1). The factors include AuNP volume (A), DPV potential range (B), ssDNA probe concentration (C), the immobilization incubation time of ssDNA probe (D), $AgNO_3$ concentration (E), $AgNO_3$ settling time (F), and the electrode potential of Ag (I). Every run was in duplicate resulting current as the response. Grey shaded columns are at constant levels since they are not statistically significant from the experimental results of the Plackett–Burman design.

No	A	B	C	D	E	F	G	H	I	J	Current (μA)	
	(μL)	(V)	(μg/mL)	(min)	(μM)	(min)	(mM)	(min)	(V)	(s)	1	2
1	40	−0.5–+0.5	1	60	200	30	15	10	−0.5	5	0.295	0.276
2	40	−1–+1	1	60	100	45	15	10	−0.5	5	2.225	2.176
3	50	−1–+1	1	60	200	30	15	10	−1	5	1.904	1.642
4	50	−0.5–+0.5	1	60	100	45	15	10	−1	5	0.433	0.384
5	40	−0.5–+0.5	1.5	30	100	45	15	10	−0.5	5	0.131	0.117
6	50	−0.5–+0.5	1.5	30	200	30	15	10	−1	5	0.004	0.002
7	50	−1–+1	1.5	30	100	45	15	10	−1	5	1.035	0.968
8	40	−1–+1	1.5	60	200	45	15	10	−1	5	1.506	0.769
9	40	−0.5–+0.5	1.5	60	100	30	15	10	−1	5	0.272	0.261
10	40	−0.5–+0.5	1	30	200	45	15	10	−1	5	0.468	0.455
11	50	−1–+1	1	30	200	45	15	10	−0.5	5	0.654	0.597
12	50	−1–+1	1.5	60	100	30	15	10	−0.5	5	2.384	1.906
13	40	−1–+1	1.5	30	200	30	15	10	−0.5	5	0.617	0.592
14	40	−1–+1	1	30	100	30	15	10	−1	5	2.960	2.503
15	50	−0.5–+0.5	1.5	60	200	45	15	10	−0.5	5	0.282	0.279
16	50	−0.5–+0.5	1	30	100	30	15	10	−0.5	5	0.154	0.149

Table S4
Analysis of variance table from the regression of experimental results using the two-level fractional factorial design in Table S3. The factors are AuNP volume (A), DPV potential range (B), ssDNA probe concentration (C), the immobilization incubation time of the ssDNA probe (D), $AgNO_3$ concentration (E), $AgNO_3$ settling time (F), and the electrode potential of Ag (I).

	df	Sum Square	Mean Square	*F*-value	*p*-value
A	1	0.183	0.183	0.894	3.54×10^{-1}
B	1	10.595	10.595	51.746	1.96×10^{-7}
C	1	1.359	1.359	6.638	1.66×10^{-2}
D	1	0.661	0.661	3.228	8.50×10^{-2}
E	1	1.873	1.873	9.15	5.85×10^{-3}
F	1	0.323	0.323	1.576	2.21×10^{-1}
I	1	0.097	0.097	0.472	4.98×10^{-1}
Residuals	24	4.914	0.205		

Table S5
Two-level full factorial design in the development of SPCE-Au with ssDNA probe. The factors include DPV potential range (B), ssDNA probe concentration (C), and incubation duration for AuNP (J). Every run was in duplicate resulting current as the response. Grey shaded columns are at constant levels since they are not statistically significant from the experiment results of the two-level fractional factorial design.

No	A (μL)	B (V)	C (μg/mL)	D (minutes)	E (μM)	F (minutes)	G (mM)	H (minutes)	I (V)	J (second)	K (hour)	Current 1	Current 2
1	40	−0.5–+0.5	1.5	60	50	30	15	10	−1	5	3.5	2.626	2.662
2	40	−0.5–+0.5	1	60	50	30	15	10	−1	5	3.5	3.148	3.336
3	40	−1–+1	1	60	50	30	15	10	−1	5	3.5	1.636	1.753
4	40	−1–+1	1.5	60	50	30	15	10	−1	5	3.5	5.567	7.792
5	40	−0.5–+0.5	1.5	60	150	30	15	10	−1	5	1	0.534	0.584
6	40	−1–+1	1.5	60	150	30	15	10	−1	5	1	0.534	0.584
7	40	−1–+1	1	60	150	30	15	10	−1	5	1	1.964	2.302
8	40	−0.5–+0.5	1	60	150	30	15	10	−1	5	3.5	3.255	3.502
9	40	−0.5–+0.5	1.5	60	150	30	15	10	−1	5	3.5	5.799	6.524
10	40	−0.5–+0.5	1.5	60	50	30	15	10	−1	5	1	5.499	5.630
11	40	−1–+1	1	60	50	30	15	10	−1	5	1	3.331	3.532
12	40	−1–+1	1	60	150	30	15	10	−1	5	3.5	4.907	5.241
13	40	−0.5–+0.5	1	60	150	30	15	10	−1	5	1	3.180	3.814
14	40	−0.5–+0.5	1	60	50	30	15	10	−1	5	1	3.339	3.905
15	40	−1–+1	1.5	60	150	30	15	10	−1	5	3.5	6.991	7.239
16	40	−1–+1	1.5	60	50	30	15	10	−1	5	1	3.143	3.367

Table S6
Analysis of variance table from the regression of experiment results using the two-level full factorial design in Table S5. B is DPV potential range, C is ssDNA probe concentration, E is $AgNO_3$ concentration, and K is the incubation duration for AuNP.

	df	Sum Square	Mean Square	*F*-value	*p*-value
B	1	1.62	1.62	0.91	3.54×10^{-1}
C	1	10.916	10.916	6.133	2.48×10^{-2}
E	1	0.032	0.032	0.018	8.96×10^{-1}
K	1	10.644	10.644	5.98	2.64×10^{-2}
Blocks	1	2.891	2.891	1.624	2.21×10^{-1}
B:C	1	4.243	4.243	2.384	1.42×10^{-1}
B:E	1	1.721	1.721	0.967	3.40×10^{-1}
B:K	1	4.683	4.683	2.631	1.24×10^{-1}
B:Blocks	1	1.524	1.524	0.856	3.69×10^{-1}
C:E	1	1.071	1.071	0.602	4.49×10^{-1}
C:K	1	18.09	18.09	10.163	5.72×10^{-3}
C:Blocks	1	0.075	0.075	0.042	8.40×10^{-1}
E:K	1	19.656	19.656	11.043	4.30×10^{-3}
E:Blocks	1	0.001	0.001	0.001	9.77×10^{-1}
K:Blocks	1	0.159	0.159	0.089	7.69×10^{-1}
Residuals	16	28.48	1.78		